Kinetic and affinity analyses of hybridization reactions between peptide nucleic acid probes and DNA targets using surface plasmon field-enhanced fluorescence spectroscopy

Hyeyoung Park
Max-Planck-Institute for Polymer Research, Ackermannweg 10, D-55128 Mainz, Germany

Andrea Germini, Stefano Sforza, Roberto Corradini, and Rosangela Marchelli
Department of Organic and Industrial Chemistry, University of Parma, Parco Area delle Scienze 17/A, 43100 Parma, Italy

Wolfgang Knoll[a)]
Max-Planck-Institute for Polymer Research, Ackermannweg 10, D-55128 Mainz, Germany

Peptide nucleic acid (PNA), a polyamide DNA mimic, has inspired the development of a variety of hybridization-based methods for the detection, quantification, purification, and characterization of nucleic acids owing to the stability of the PNA/DNA duplex. In this work, PNA probes complementary to a specific sequence of Roundup Ready® soybean were immobilized onto a sensor surface via a self-assembled matrix employing streptavidin/biotin binding. The specific hybridization of PNA and DNA has been monitored by applying the chromophore-labeled DNA target oligonucleotides to the PNA modified Au sensor surface in real time using surface plasmon field-enhanced fluorescence spectroscopy. The authors demonstrate three kinds of experiments called global, titration, and kinetic analyses for the determination of rate constants for the association (k_{on}) and dissociation processes (k_{off}), and the affinity constant (K_A) of the PNA/DNA duplex formation by fitting the data to a simple Langmuir model. Discrimination of a single base mismatched DNA (15mer) target on a 15mer PNA probe was documented, with a difference of the affinity constant of two orders of magnitude. Finally, the affinity constant for the hybridization of a long polymerase chain reaction product (169mer) obtained by amplification of DNA extracted from genetically modified soybean reference material has been determined by a kinetic-titration analysis. The results show the influence of a Coulomb barrier at high target surface coverage even for the hybridization to PNA at low ionic strength. © 2006 American Vacuum Society.
[DOI: 10.1116/1.2365386]

I. INTRODUCTION

Peptide nucleic acids (PNAs) will play an important role in improving existing and developing novel techniques for DNA hybridization-based sensing platforms with better sequence discrimination in genetic diagnostics and molecular biology.[1] Several key issues suggest the use of PNA rather than DNA probes for sensor-based hybridization. Firstly, the hybrid stability as measured by the melting temperature (T_m) of PNA/DNA duplexes displays, in general, a slightly higher value than the corresponding DNA/DNA duplexes at physiological ionic strength.[2] Secondly, by virtue of the fact that PNA has a noncharged pseudopeptide backbone, its physicochemical properties differ significantly from polyanionic oligonucleotides. The stability of PNA/DNA complexes in solution is therefore almost insensitive to the ionic strength (which is, in part, due to the noncharged PNA backbone).[3]

Biomolecular interactions have been analyzed based on electrochemical data,[4] atomic force microscopy studies,[5] quartz crystal microbalance measurements,[6] and by other techniques. Among the optical methods, surface plasmon resonance (SPR) spectroscopy can be used to monitor in real time the interaction between molecules at the surface of a thin metal film, typically gold. Excitation of a surface plasmon mode occurs if polarized light is reflected off the interface between a thin metal film and a dielectric medium, e.g., in the Kretschmann geometry, cf. Fig. 1, at the resonance angle which is given by the energy/momentum matching condition between the photon and surface plasmon modes.[7] The alternating electromagnetic field of the light causes oscillations of the nearly free electron gas in the metal. These oscillations produce an evanescent wave that is spatially confined, decaying in an exponential way normal to the surface. In surface plasmon field-enhanced fluorescence spectroscopy (SPFS) we use such surface plasmon waves to excite chromophore-labeled analyte target molecules and monitor their fluorescence intensity in real time during hybridization.[8] The nature of the evanescent field of the surface plasmon mode leads to an excitation probability that is also exponentially decaying away from the interface.[9] However, should the chromophore be placed too close to the metal substrate, Förster energy transfer mechanisms would result in an undesired loss of emission probability. Taking both effects into account, the chromophore-labeled analyte

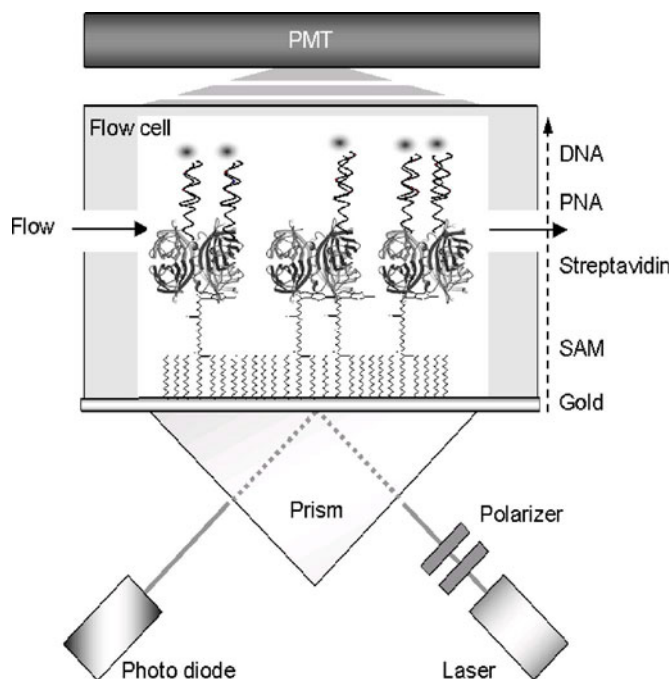[a)]Electronic mail: knoll@mpip-mainz.mpg.de

FIG. 1. Illustration of the self-assembled sensor matrix in a flow cell for surface plasmon fluorescence spectroscopy.

should be placed within a matrix layer of approximately 20–100 nm away from the Au sensor surface.[10] In order to achieve an optimized fluorescence signal, a well-established architecture was used for the sensor surface, which is schematically given in Fig. 1.[11]

Many examples for the kinetic analysis of biomolecular interaction processes on a sensor surface using SPFS have been reported.[12–18] Most of these studies were based on a simple bimolecular interaction scheme:

PNA probe, surface

$$+ \text{DNA target, solution} \underset{k_{\text{off}}}{\overset{k_{\text{on}}}{\rightleftharpoons}} \text{PNA/DNA duplex, surface.}$$
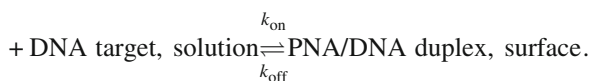
The binding of fluorophore-labeled DNA targets to PNA probes results in a change of the thickness, reflectivity, and fluorescence intensity. The association rate constant k_{on} and the dissociation rate constant k_{off} are obtained by separately fitting selected sections of the data of the association and dissociation phases, respectively.

We aimed at determining the rate constants for hybridization reactions especially at fixed experimental conditions such as constant temperature, flow rate, target solution volume, etc., by using SPFS. Global analysis is a very convenient approach and promises stringent results of an entire data set with different target concentrations in a short time. On the other hand, titration experiments measure the surface coverage at equilibrium with the bulk concentration after increasing or decreasing the target concentration in the bulk solution. Here, we also present kinetic-titration experiments with supplementary rinsing steps. In addition, a single-exponential kinetic analysis provides rate constants at a cer-

tain concentration. With these approaches, the hybridization between PNA and DNA has been evaluated with rate and affinity constants resulting from the three different experiments. The PNA probes used were designed so as to be complementary to a tract of Monsanto's Roundup Ready® soybean, since the present work is a part of a general project aimed at developing tools for the detection of genetically modified organisms (GMOs) in food.[19–21]

Finally, an example for the detection of DNA amplicons from GMOs in food was studied quantitatively by a titration analysis. To this end, target DNA (RR-169, fully matched to a PNA probe in the middle part of its sequence) was amplified by polymerase chain reaction (PCR) using a template gene extracted from Roundup Ready® soybean.
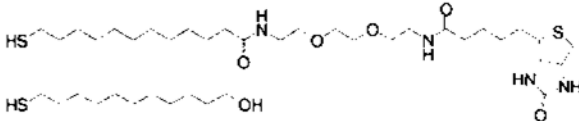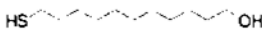
II. EXPERIMENT

A. PNA synthesis

All solvents used for high-performance liquid chromatography (HPLC) were of chromatographic grade. Ultrapure water was produced by a millipore Alpha-Q purification module. *N*-methylpyrrolidone was from Fluka.

The PNA probes were synthesized using solid-phase synthesis with a 433A peptide synthesizer (Applied Biosystems) with the BOC strategy and *O*-(1*H*-7-azabenzotriazolyl)-*N*,*N*,*N*′,*N*′-tetramethyluronium hexafluorophosphate (Aldrich) coupling and *N*,*N*-diisopropylethylamine (Aldrich) as base, using commercially available PNA monomers (Applied Biosystems) and (4-methylbenhydryl)amine resin (Novabiochem) as solid support as described in a previous work.[22] After the PNA part was completed, two coupling steps were performed using the protected linker [2-(*N*-Boc-2-amioethoxy)ethoxyacetic acid dicyclohexylammonium salt (AEEA, Applied Biosystems)] and a coupling step using biotin (Aldrich). Cleavage of the PNA from the resins was then carried out manually using a mixture of a trifluoroacetic acid (TFA) and trifluoromethanesulfonic acid: thioanisole: *m*-cresol 6:2:1:1. Swelling, downloading, and cleaving of the PNAs from the resin were done manually. The crude product was purified by reversed phase HPLC using a Phenomenex C18 peptide column (3 μm, 250 $\times$ 10 mm^2) with a binary gradient (flow rate: 4 mL/min); eluent A: water/TFA =100:0.1; eluent B: water/acetonitrile/TFA=60:40:0.1; and UV detector (260 nm). The purified product was then identified by mass spectrometry (Micromass ZMD). Using electroscopy ionization mass spectrometry, the estimated mass for M^+ 4609.6 was found to be 4609.8. The sequences of all probes and targets are given in Table I.

B. Surface plasmon field-enhanced fluorescence spectroscopy (SPFS)

A HeNe laser beam (5 mW, λ=632.8 nm, Uniphase) passes through a chopper that is connected to a lock-in amplifier (EG&G) in order to allow for reduced noise and daylight independent measurements of the reflected intensity. The intensity and polarization of the incident light were adjusted by two polarizers (Glan-Thompson). The exposure

TABLE I. Molecular structures of the materials used in this study.

| Mixed SAM | Biotinylated thiol | |
| | Spacer thiol | |

Probe — PNA — Biotin -AEEA -AEEA -TGCTAGAGTCAGCTT -NH$_2$

*AEEA = 2-(2-aminoethoxy)ethoxyacetic acid

Targets

RR-15 — Cy5 –5' AAGCTGACTCTAGCA-3'

RR- mis-15 [a] — Cy5 –5' AAGCTG**G**CTCTAGCA-3'

RR-125 [b] — Cy5 –5' CATTCATTTGGAGAGGACACGCTGAC
AAGCTGACTCTAGCAGATCTTTCAAGAAT
GGCACAAATTAACAACATGGCACAAGGG
ATACAAACCCTTAATCCCAATTCCAATTT
CCATAAACCCCA -3'

RR-169 [b] — Cy5 –5' ATCCCACTATCCTTCGCAAGACCCT
TCCTCTATATAAGGAAGTTCATTTCATT
TGGAGAGGACACGCTGAC<u>AAGCTGACT
CTAGCA</u>GATCTTTCAAGAATGGCACAA
ATTAACAACATGGCTCAAGGGATACAA
ACCCTTAATCCCAATTCCAATTTCCATA
AACCC

[a]Boldface G is the mismatching base.
[b]Underlined base pairs are complementary to the PNA probe.

time was controlled by placing a shutter in front of the sample in order to minimize any photobleaching of the fluorescent dyes. Typically, the shutter was open for 5 s and closed for 3 min, except for the global analysis. The incident laser is reflected off the base plane of the coupling prism (90°, LaSFN9, Schott), and the reflected intensity is focused by a lens ($f=50$ mm, Owis) for detection by a photodiode. The sample is mounted onto a two-phase goniometer (Huber) that can be rotated in $\Delta\theta=0.001°$ steps. In order to detect the fluorescence emission of the sample, a collecting lens focuses the emitted light through an interference filter ($\lambda=670\pm2$ nm, LOT) into a photomultiplier tube (Hamamatsu), which is mounted towards the backside of the sample (Fig. 1).

C. Self-assembled sensor matrix

LaSFN9 (Schott, $n=1.85$ at $\lambda=633$ nm) glass substrates were cleaned carefully by ultrasonication in 1% detergent solution (Hellmanex) and rinsed with Milli-Q water. After drying the glass, a layer of gold was deposited (approximately 50 nm) by thermal evaporation (Edwards, $p < 10^{-6}$ mbar). The sensor architecture is given in Fig. 1. For the preparation of the self-assembled monolayers (SAMs), the gold surface was incubated overnight in a binary mixed thiol solution of a biotinylated thiol (biotinamino-

capronacid-amidodioctyl-mercaptopropionamide, Table I) and a spacer thiol (11-mercapto-1-undecanol, Aldrich, Table I) at a molar ratio of 1:9 and a total concentration of 0.5 mM in absolute ethanol (Aldrich). Then, the streptavidin solution (1 μM, Kem-En-Tec Diagnostics) was rinsed through the flow cell system (homemade, 500 μL total volume including the Tygon tubing) in order to allow for binding to the self-assembled thiol layer at a flow rate of 10 μL/s. Subsequently, biotinylated PNAs (500 nM) were immobilized on the streptavidin layer as catcher probes via the streptavidin/biotin binding. The sequences of the PNAs were designed especially for the detection of the Roundup Ready® DNA targets (RR-169, a PCR product with 169 base pairs). The targets for sensing DNA oligonucleotides (RR-15 and RR-mis-15) were purchased from MWG-Biotech. All molecular structures are shown in Table I.

D. PCR products

Amplification was carried out with the primers (MWG-Biotech) GM 08: Cy5-5′-TGG GGT TTA TGG AAA TTG GAA-3′ and ATC CCA CTA TCC TTC GCA AGA-3′, respectively. 50 μL of a mixture of Taq polymerase (5 u, Qiagen), buffer, primers (0.5 μM), dNTPs (0.2 mM, Fermentas), template (150 ng, extracted from soybean certified reference material, Fluka), and sterilized water were pre-

pared. Using a thermocycler (Biometra) 40 PCR cycles are run as follows: denaturation at 95 °C for 50 s, annealing at 58 °C for 50 s, and elongation at 72 °C for 1 min. The PCR products were analyzed by agarose gel [2%, 0.5×TBE (tris/borate/ethylenediamine tetra-acetic acid) buffer] electrophoresis at 50 mA for 2 h in 0.5×TBE buffer stained with ethidium bromide. The amplified PCR products were purified by ethanol precipitation by mixing 50 μL PCR, 125 μL ethanol, and 5 μL sodium acetate (3M, Sigma) and incubating at −20 °C for 6 h. The PCR products were collected by centrifugation at 20 000 rpm. In order to prepare single-stranded target DNA, double-stranded PCR products in 10 mM phosphate buffer were denatured at 95 °C for 10 min, then quenched in an ice bath in order to prevent rehybridization. The concentration of the PCR product was calculated by UV-vis absorbance at λ=650 nm using an extinction coefficient of Cy5 of ε=250 000 cm^{-1} M^{-1}.

E. PNA/DNA hybridization

The angle of incidence was fixed at θ=55.5° for monitoring the PNA/DNA hybridization. Kinetics curves were recorded in both the reflectivity and fluorescence modes, starting with a measurement of the fluorescence background for a few minutes as a function of time. All the experiments were performed with 1 mL for each target concentration using the same flow cell with an inlet and outlet and a closed loop circulation at room temperature (24±1 °C) and at a flow rate of 10 μL/s.

For the global analysis, Cy-5 labeled oligonucleotide target solutions (varying in concentration typically from 1 nM up to 200 nM) were introduced into the flow cell for the association and were allowed to interact with the PNA functionalized sensor surface for 10 min. After that the dissociation was followed for 10 min by rinsing with fresh buffer solution (10 mM phosphate buffer solution) for each measurement. The surfaces could be fully regenerated by treatment with 10 mM NaOH in order to remove the remaining bound target DNA for another analysis cycle at the same sensor surface.

For the titration experiment, a 1 nM solution in 10 mM phosphate buffer of target was injected after recording the background fluorescence, and the increase in fluorescence intensity was measured as a function of time until the equilibrium surface coverage was reached. Next, target DNA solutions of 5, 10, 20, 50, and 100 nM, respectively, were applied consecutively.

The kinetic-titration experiment was performed as follows: a 1 nM solution of target was injected, and the increase in fluorescence intensity was measured as a function of time until the surface coverage reached equilibrium. Then, the injection of 5–10 nM target solutions resulted in a correspondingly higher equilibrium coverage. After equilibrium the surface was rinsed with pure 10 mM phosphate buffer solution for typically 1 h. Then, the next higher target concentrations were applied, with rinsing steps of phosphate buffer in be-

tween. An angular scan was taken at each equilibrium state with the bulk solution in the flow cell and shortly after rinsing the cell with pure buffer.

Each single-exponential analysis was completed by applying a 50 nM target solution (RR-15 and RR-mis-15) until equilibrium was reached, followed by an extended rinsing step.

III. RESULTS AND DISCUSSION

A. PNA probe immobilization on a self-assembled sensor matrix

Briefly, the surface architecture on the sensor substrate was prepared by a self-assembly strategy in the following way: a thermally deposited approximately 50 nm thick gold layer was functionalized by a mixed self-assembled monolayer of a biotinylated thiol derivative and a shorter hydroxyl-terminated alkyl chain thiol, resulting in a hydrophilic surface which allows for the formation of a monolayer of streptavidin as a generic binding matrix and at the same time minimizes nonspecific adsorption. The immobilization of the biotinylated PNA was then achieved on the streptavidin surface by the streptavidin/biotin binding (K_A=10$^{14}M^{-1}$).

The thiol mixture is composed of two different alkane thiols: one terminated with a biotin group for subsequent streptavidin binding (10 mol %), and a shorter thiol (90 mol %) terminated with a hydroxyl group that acts as a spacer to dilute the biotinylated species, in order to control the surface density and to minimize nonspecific adsorption of analyte (target) molecules.[23] Immobilization of both the streptavidin to the SAM layer and the PNA probe to the streptavidin layer was measured by SPR [Fig. 2(a)]. The adsorption kinetics was fast and the immobilized probe layer was stable in buffer solution for about 200 h. It is worth noting that the sensor surface is still robust and gives reproducible results even after several regenerations (by rinsing with 10 mM NaOH solution). Before and after the adsorption process, the mixed thiols, the streptavidin, and the PNA probe layers were characterized by fitting the SPR scan curves using the Fresnel simulation software WINSPALL 2.0. The calculated thicknesses of gold, the mixed thiols (n=1.5), the streptavidin (n=1.45), and the PNA probe (n=1.45) layers were 57.5, 1.5, 3.3, and 1.3 nm, respectively [Fig. 2(b)]. This architecture ensures a moderate catcher probe density of about 2.5×10^{12} probes/cm^2, because on average 1.3 probe strands can be attached to the streptavidin layer,[24] thus reducing any potential cross talk between individual reaction sites during hybridization.

B. Kinetics and affinities of PNA/RR-15 hybridization

1. Global analysis by SPFS

If the target solution is applied to a probe-modified sensor surface, it is difficult to observe a reasonably strong response by SPR because duplex formation with oligomeric DNA does not generate a significant change in the optical thickness. However, SPFS measurements demonstrated a high
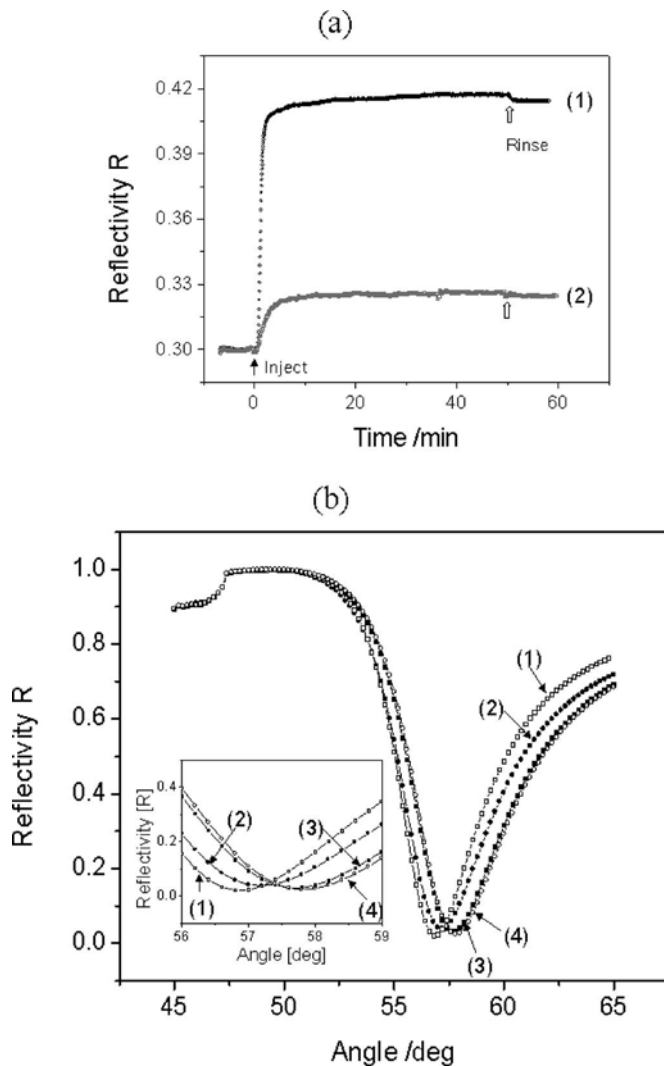
FIG. 2. (a) Kinetic SPR curves taken at $\theta = 55.7°$ (at this angle, the reflectivity changes approximately linearly with the bound optical mass): (1) streptavidin binding to a biotinylated thiol SAM and (2) biotinylated PNA probes binding to a streptavidin layer. (b) Angular scan curves of the reflectivity R: (1) reference gold, (2) mixed SAMs (full circles), (3) streptavidin layers, and (4) PNA probe layers (open circles). The inset shows a zoom in on the angles between 56° and 59°.

sensitivity for monitoring binding events between immobilized PNA and chromophore-labeled target DNA even at concentrations in the femtomolar range.[25] This fluorescence intensity carries kinetic information of hybridization and can be analyzed in terms of the corresponding rate constants for association (k_{on}) and dissociation (k_{off}), and the affinity constant (K_A).

Figure 3(a) shows experimental data for the global analysis taken at $\theta = 55.7°$ at different concentrations of the complementary DNA RR-15 with PNA at low ionic strength (10 mM phosphate) buffer solution using the same sensor surface each time. Starting for a short time with the base line measurement [the intensity of the base line gives I_0 in Eq. (1)], solutions of varying concentrations of DNA targets were injected and circulated for 10 min approximately in order to follow the association process as measured by the
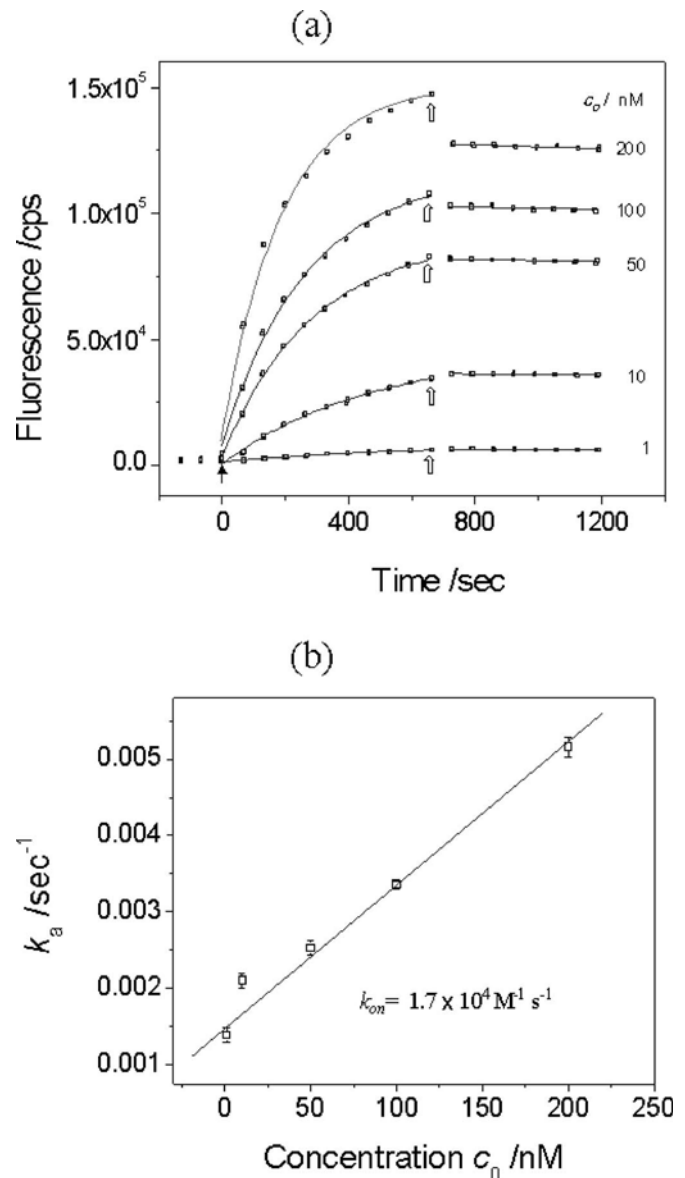

FIG. 3. (a) Global analysis of the association and dissociation phases (taken at $\theta = 55.7°$) of PNA/DNA RR-15 hybridization in a solution containing 10 mM phosphate buffer solution. The open squares are data points collected every 1 min. The solid arrow at $t = 0$ indicates the injection of the target solutions of different concentrations for the recording of the association phase. The open arrows point to the beginning of the rinsing step for the dissociation phase. The solid lines are the best fit to a Langmuir model. The bulk concentrations are 1, 10, 50, 100, and 200 nM of RR-15 target solutions, as indicated. (b) k_a obtained from fitting the data (open squares) of (a) as a function of target concentration c_0. The solid straight line is a linear fit. (c) Global analysis of the association and dissociation phases (taken at $\theta = 55.7°$) of PNA/DNA RR-mis-15 hybridization in a solution containing 10 mM phosphate buffer solution. (d) k_a obtained from fitting the data (open squares) of (c) as a function of target concentration c_0. Typical R^2 after fitting is 0.999.

increase in fluorescence intensity. Then the cell was rinsed with fresh buffer solution for 10 min in order to measure the dissociation process. Based on the Langmuir model the increase of the fluorescence intensity as a function of time is described by a simple bimolecular reaction as follows:

$$I_{fl}(t) = (I_{max} - I_0)(1 - \exp(- (k_{on}c_0 + k_{off})t)), \tag{1}$$

with I_{max} being the maximum fluorescence intensity from surface-bound duplexes at c_0, I_0 is the initial background fluorescence, and c_0 is the bulk solution concentration in the global analysis.

The association kinetics is quantified with respect to the concentration dependence. Fitting the association phase data recorded from 0 to 670 s with Eq. (1), the rate constants $k_a = k_{on}c_0 + k_{off}$ were obtained individually at different target concentrations. The k_a values increased as the concentration increased, as shown in Fig. 3(b). The k_{on} value was thus obtained from the slope of the k_a versus target concentration plot and calculated to be $k_{on} = 1.7 \times 10^4 M^{-1} s^{-1}$. As can be seen from Fig. 3(b) the noise in the data, unfortunately, does not allow for a reliable determination of k_{off} from k_a at $c_0 = 0$. Moreover, for a hybrid as stable as the fully matched double strand between the PNA probe and the 15mer DNA target (RR-15), only a very small decrease of the fluorescence intensity by the dissociating target can be found during the 10 min rinsing phase of the global analysis. This clearly limits, for very stable hybrids, the quantification of the full set of kinetic parameters by this approach.

However, by introducing a single mismatch in the base sequence of the target (RR-mis-15, cf. Table I) the duplex is largely destabilized and, hence, the dissociation sufficiently enhanced, thus, leading to a measurable loss of fluorescence intensity even within the 10 min of the rinsing phase of the global analysis. This is shown in Fig. 3(c). The rate constant k_a for the RR-mis-15 target is plotted in Fig. 3(d). From the slope, k_{on} is obtained to be $k_{on} = 3.1 \times 10^3 M^{-1} s^{-1}$, significantly lower than for the full match RR-15 case.

The time-dependent dissociation is described by

$$I_{fl}(t) = (I_{max} - I_0)\exp(- k_{off}t). \tag{2}$$

Note that after exchanging the buffer solution a drop in the fluorescence intensity can be observed at the starting point of the dissociation phase, which accounts for 5.2%, 13.4%, and 19.7% of the fluorescence intensity at $c_0 = 100$, 200, and 500 nM, respectively. This contribution originates from free fluorophores (targets) in the solution near the surface that are rinsed out during the exchange with pure buffer solution.

From the decrease of the fluorescence intensity during the following rinsing process, the dissociation rate was determined to be $k_{off} = 2.5 \times 10^{-4} s^{-1}$, which is the average value of each k_{off} value by fitting each dissociation part of the measurement (during rinsing) using Eq. (2) as shown in Fig. 3(c). Thus the affinity constant, K_A ($K_A = k_{on}/k_{off}$), is found to be $K_A = 1.2 \times 10^7 M^{-1}$ for the RR-mis-15 target.

2. Titration measurements

An alternative measurement for the quantitative study of the hybridization process is a titration experiment. According to the Langmuir model the amount of analyte adsorbed at a given temperature to the binding sites is determined by the equilibrium between free and bound analyte molecules, i.e., by the surface coverage Θ, corresponding to the fluorescence

intensity, I_{max}. This surface coverage depends on the affinity constant K_A and on the bulk concentration c_0. It is possible to monitor the Langmuir adsorption isotherm by performing experiments in which surface saturation is reached by a stepwise increase (or decrease) of the bulk concentration. The general procedure involves the injection of the analyte solution at low concentration and allowing for the adsorption process to reach equilibrium. This process is repeated with target solutions of higher concentrations until the surface is fully covered by the analyte. The surface coverage is described by

$$I_{fl}(c_0) \propto \Theta(c_0) = \frac{c_0 K_A}{1 + c_o K_A}. \tag{3}$$

In practice, the surface coverage $\Theta(c_0)$ is determined by scaling the detected signal intensity $I_{fl}(c_0)$ to that of a fully saturated surface. Figure 4 shows the titration experiment for PNA/DNA RR-15 hybridization monitored at a fixed angle of incidence of $\theta = 55.7°$. After the background fluorescence was recorded for a few minutes, a 1 nM solution of RR-15 was injected and the increase in fluorescence intensity was measured as a function of time until the equilibrium between the bulk concentration and the corresponding surface coverage was reached. Next, the injection of 5, 10, 20, 50, and 100 nM target solutions, respectively, resulted in correspondingly higher equilibrium surface coverages with the higher equivalent fluorescence intensities as shown in Fig. 4(a). In addition, a series of angular scans was taken after the surface coverage reached a new equilibrium for each new bulk concentration, as shown in Fig. 4(b). Several features are noteworthy: (1) No significant shift of the surface plasmon minimum angle was observed (the various reflectivity curves are virtually superimposed) indicating the negligible increase in the optical thickness upon forming the PNA/DNA duplex. (2) The fluorescence from the bulk solution excited by light transmitted through the 50 nm Au substrate at 45°, below the critical angle ($\theta_c = 47.3°$), was measured at each concentration. As demonstrated in Fig. 5(a), this intensity is a linear function of the target concentration (from 1 to 100 nM) due to the direct excitation of the fluorophores in the bulk solution.

The Langmuir isotherm curve was constructed from the data taken at the angle of maximum intensity of the angular scans (after rinsing for a short time) as a function of target concentration. In Fig. 5(b) and 5(c) the open squares are the data from angular scans [Fig. 4(b)] and the solid line is a simulated Langmuir fit using Eq. (3). Figure 5(c) corresponds to a linearized Langmuir isotherm [Eq. (4)] according to a modification of Eq. (3) with an affinity constant of $K_A = 1.7 \times 10^8 M^{-1}$:

$$\frac{c_0}{I_{fl}} \propto \frac{1}{K_A} + c_0. \tag{4}$$

By analyzing the dissociation phase of Fig. 4(a) (and of Fig. 6), a dissociation rate constant of $k_{off} = 1.7 \times 10^{-5} s^{-1}$ can
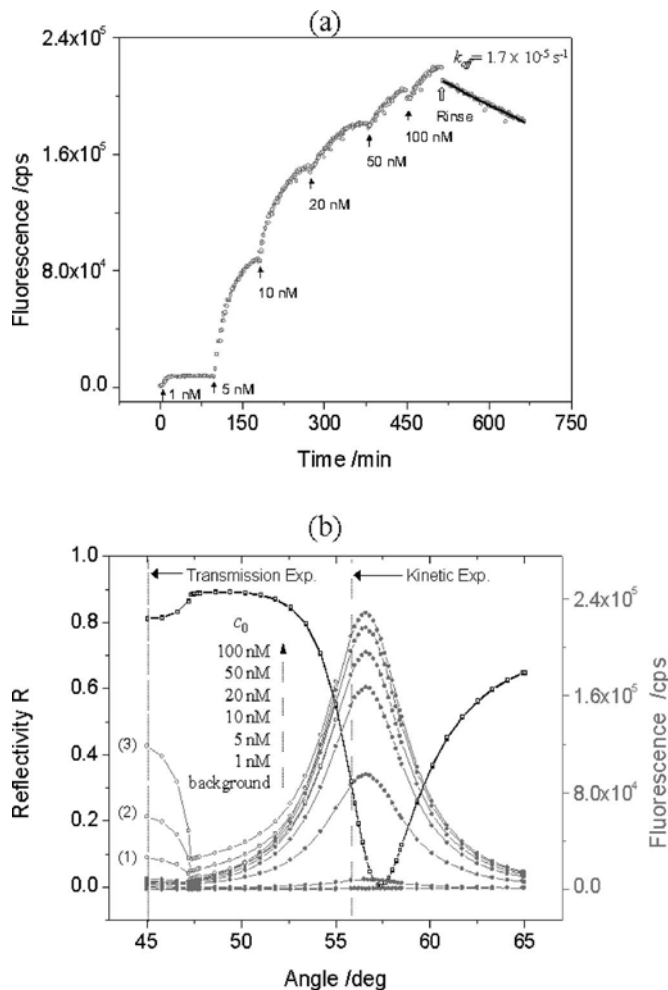
FIG. 4. (a) Titration curves for PNA/DNA RR-15 hybridization at $\theta=55.7°$. The concentration of the target DNA RR-15 was stepwise increased from 1 to 5, 10, 20, 50, and 100 nM, respectively, in 10 mM phosphate buffer solution. The open circles are data points collected every 3 min. The solid arrows indicate the injection of the target solution. The fluorescence was recorded until the saturation intensity was reached. After the recording of the 100 nM sample the dissociation process was started by rinsing with pure buffer (open arrow). The solid line is a Langmuir fit to the dissociation data. (b) Angular scans taken after saturation was reached for the 1, 5, 10, 20, 50, and 100 nM target solutions, respectively, together with the background fluorescence intensity. The open squares are reflectivities. Note that there is no significant plasmon minimum angle shift by forming a PNA/DNA duplex. Angular fluorescence curves were taken before (open symbols) and after rinsing (full symbols) the flow cell with pure buffer following the equilibrium binding of targets from solutions: (1) 20 nM, (2) 50 nM, and (3) 100 nM.

FIG. 5. (a) Fluorescence intensity measured at $\theta=45°$, i.e., below the critical angle, giving information of the bulk concentration c_0. (b) Plots (open squares) of the maximum fluorescence intensity ($\theta=56.6°$) taken from Fig. 4(b) versus target concentration c_0. The gray curve corresponds to the fit by a Langmuir isotherm. (c) Linearized Langmuir isotherm of the data of (b), yielding $K_A=1.7\times10^8 M^{-1}$. Typical R^2 after fitting is 0.999.

be calculated. Together with the k_{on} value derived from the association phase of the global analysis, this leads to an affinity constant of $K_A=1\times10^9 M^{-1}$.

It is interesting to compare this affinity constant with that determined from the titration analysis. The K_A value obtained from the global analysis is approximately six times higher than that of the titration experiment. We attribute this effect to the increasing surface charge density upon hybridization of DNA targets: starting with an (empty) uncharged PNA probe matrix at the sensor surface, each bound target oligonucleot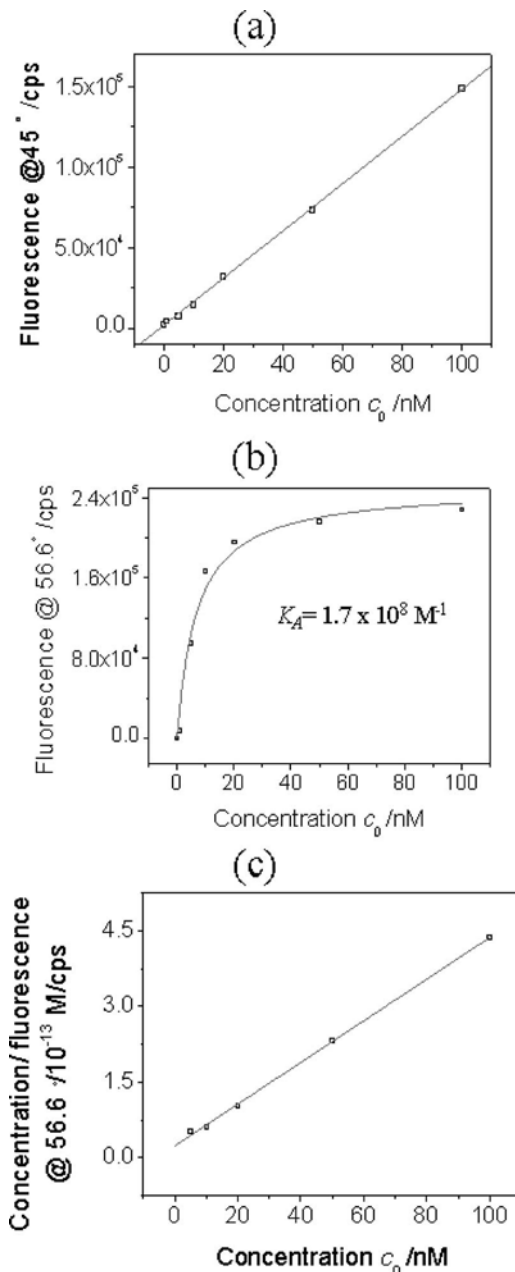ide adds 15 charges to the interface. As the coverage increases, this surface charge density generates a successively increasing repulsive Coulomb barrier for further target binding to the still free binding sites which are, however, cross talking with the neighboring (charged) hybrids. In earlier studies, we demonstrated that this effect could be reduced when working at high ionic strength or by diluting the probe density of the sensor matrix, thus increasing the average distance between individual hybridization sites.[25] The target-binding-induced generation of a repulsive Coulomb
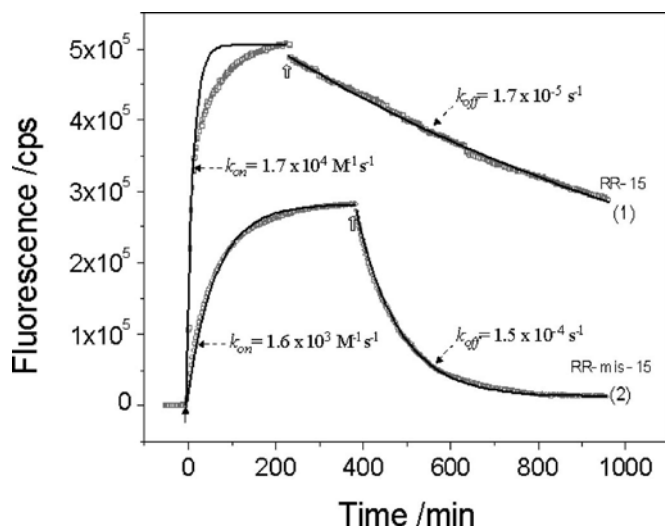
FIG. 6. Hybridization kinetics recorded at $\theta = 55.7°$ for (1) PNA/DNA RR-15 (50 nM, open squares). The solid curves (1) are fits to the data by a Langmuir model (R^2 values after fitting for the k_{on} and k_{off} are 0.770 and 0.997, respectively). (2) Kinetic run for the discrimination of a single mismatch hybridization: PNA/DNA RR-mis-15 (50 nM, open circles) with association and dissociation phases (solid curves are again Langmuir fit; R^2 values after fitting for the k_{on} and k_{off} are 0.991 and 0.998, respectively).

barrier also reduces the apparent affinity K_A measured in a titration experiment [cf. Fig. 4(a) and the corresponding discussion].

In the global analysis, on the other hand, the catcher probe matrix is regenerated for each separate run starting each time with an empty uncharged matrix. Only the first few minutes are observed during hybridization to reach a surface coverage that does not exceed typically 30% of the full monolayer capacity, and hence is less influenced by the buildup of a Coulomb barrier. Thus, the global analysis measures a more reliable affinity constant with less cross talk between the bound targets at the interface.

C. Kinetic analysis of PNA/RR-15 and RR-mis-15 hybridizations

The SPFS technique is sensitive and reproducible enough to not only obtain kinetic and affinity data discussed above but also to detect the effect of one base mismatch of a nucleic acid target on the PNA/DNA hybridization process. For this purpose, and to demonstrate the potential (and difficulties) of a single kinetic experiment, the binding kinetics between PNA and DNA RR-15 were measured at a target concentration of $c_0 = 50$ nM. The analysis of this experiment is also based on the simple Langmuir model. By introducing the RR-15 target DNA solution into the cell and circulating it until saturation of the fluorescence signal from the PNA sensor surface was reached, the association kinetics was measured. Then the dissociation process was triggered by switching to a 10 mM phosphate buffer solution (Fig. 6). By using a single exponential Langmuir fit, the obtained rate constants are $k_{on} = 1.7 \times 10^4 M^{-1} s^{-1}$ and $k_{off} = 1.7 \times 10^{-5} s^{-1}$, and the resulting affinity constant is $K_A = 1.0 \times 10^9 M^{-1}$. As one can see from Fig. 6(1) the high k_{on} value is obtained by fitting only

the early stage (first 10 min) of the association process. The k_{on} and the K_A values thus obtained are in good agreement with the K_A value derived from the association phase in the global analysis [Fig. 3(b)]. One can further see from the association phase in Fig. 6(1) that, for high coverage, the buildup of the Coulomb barriers leads to a slowing down of the hybridization reaction, thus resulting in an increasing deviation from the single-exponential behavior expected for a Langmuir adsorption.

For the detection of a point mutation, DNA RR-mis-15 (50 nM) was hybridized to the PNA using the same conditions. As plotted in Fig. 6(2), the rate constant of the association phase is considerably lower than that of the fully complementary hybrid with $k_{on} = 1.6 \times 10^3 M^{-1} s^{-1}$. In addition, the dissociation rate ($k_{off} = 1.5 \times 10^{-4} s^{-1}$) is faster compared to the fully matched duplex. As a consequence, the affinity constant is determined to be $K_A = 1.1 \times 10^7 M^{-1}$, i.e., about two orders of magnitude lower. This indicates that good discrimination is possible for a point mutation using this sensor matrix. Since in this experiment the equilibrium coverage is still significantly below a full monolayer, the Coulomb barrier is not so strong yet and, hence, the kinetics of association and dissociation are well described by a single-exponential fit.

The obtained kinetic rate constants for the association $k_{on} = 1.6 \times 10^3 M^{-1} s^{-1}$ and dissociation $k_{off} = 1.5 \times 10^{-4} s^{-1}$ are also reasonably close to the values obtained from the global analysis ($k_{on} = 3.1 \times 10^3 M^{-1} s^{-1}$ and $k_{off} = 2.5 \times 10^{-4} s^{-1}$, respectively) with the latter being, however, a much faster approach.

D. Detection of PCR amplicons from genetically modified soybean

The detection of long DNA fragments obtained by PCR amplification from genetically modified soybean is also possible using SPFS both in the kinetic and the titration mode. PCR is based on a sequence-specific hybridization of two primers to the template DNA.[19,20] One primer was modified with Cy5 for fluorescence detection of the target strand. Purified PCRs are originally double-stranded DNAs. In order to hybridize with PNA, a melt-quench protocol was developed[26]: The PCR products are heated to $T = 95$ °C and then quickly quenched into a low ionic strength buffer containing only 10 mM phosphate at 0 °C. This results in a Coulomb repulsion in solution between the individual single strands, sufficiently strong to prevent (rapid) rehybridization of the complementary strands.

With the target strands being fluorescently labeled, one can perform a hybridization experiment at a fixed angle of observation in the kinetic mode or, after equilibrium is established, in the angular mode of SPFS. Figure 7 shows a titration experiment in detail. After the background fluorescence was recorded as a function of the angle of incidence, a 1 nM solution of RR-169 (Table I) was injected, and after equilibrium between the bulk concentration and the corresponding surface coverage was reached, the next angular scan was recorded (Fig. 7). Next, the injection of 5, 10, 20, and
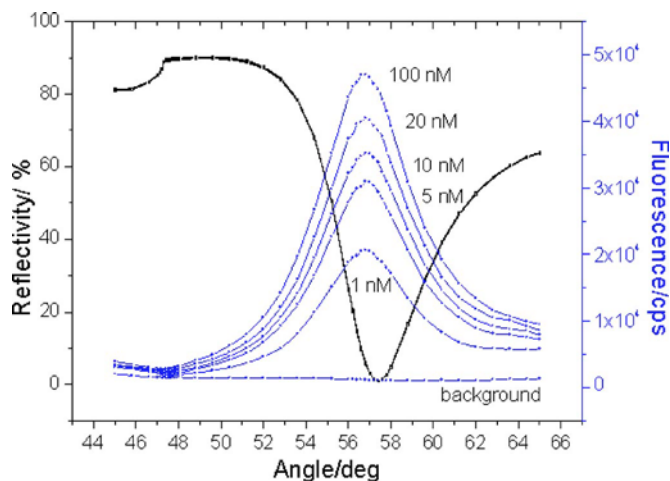
FIG. 7. Angular scans for PNA/DNA RR-169 hybridization taken in 10 mM phosphate buffer after saturation of the fluorescence was reached for 1, 5, 10, 20, and 100 nM target solutions, respectively, together with background fluorescence intensity recorded after rinsing. Typical R^2 after fitting is 0.999.

FIG. 8. Maximum fluorescence intensity [taken from Fig. 7(b) at $\theta = 57°$] vs target concentration. The full curve corresponds to a fit according to the Langmuir isotherm with $K_A = 3.8 \times 10^8 M^{-1}$. Typical R^2 after fitting is 0.999.

100 nM target solutions resulted in correspondingly higher equilibrium surface coverages with the equivalent higher fluorescence intensities. Figure 8 shows the analysis of the intensities at equilibrium surface coverages from Fig. 7. The fluorescence intensities at $\theta = 57°$ are plotted as a function of the corresponding bulk concentration. The fit to the experimental data gives the affinity constant $K_A = 3.810^8 M^{-1}$, corresponding to a half-saturation concentration of $K_d = 2.6$ nM.

It is interesting to compare this value with the one determined for slightly shorter amplicons, i.e., the RR-125 strands,[12] which were found to have virtually the identical affinity value, $K_A = 3.7 \times 10^8 M^{-1}$, and to the value of the short recognition sequence of only 15 nucleotides, i.e., $K_A = 1.7 \times 10^8 M^{-1}$ (cf. Fig. 5). Within experimental error all three values are identical, indicating that the length of the target oligonucleotide has only a minor effect on the hybridization affinities. We should mention, however, that with increasing degree of binding (coverage) of the RR-169 amplicons to the PNA catcher matrix a rather pronounced effect on the association rate is seen [as it was found in the case of the RR-125 (Ref. 12)], slowing down the hybridization process considerably (data not shown).

IV. CONCLUSIONS

SPFS is shown to allow for an in depth study of the hybridization reaction between surface attached PNA and DNA targets from solution. The optimized PNA sensor matrix constructed via SAM strategies allowed for kinetic measurements as well as for a quantitative determination of affinity constants. Moreover, it provided sufficient sensitivity to distinguish a single base mismatch in the hybridization of chromophore-labeled DNA targets. The biomolecular interaction between PNA and DNA was analyzed by three different experiments using a simple Langmuir model.

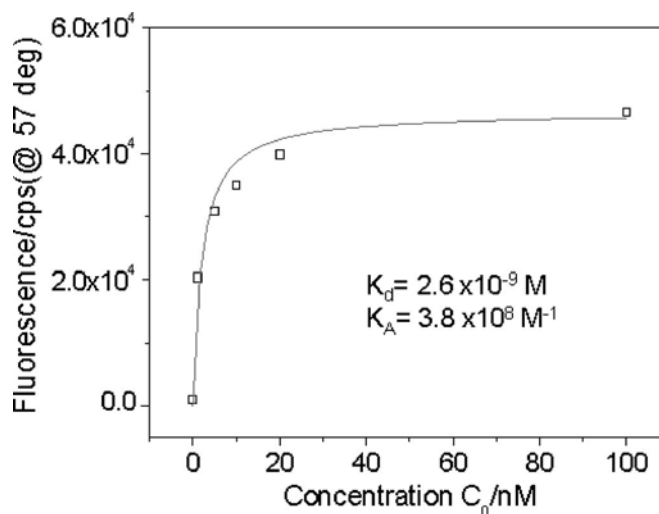The global analysis turned out to be the fastest and most reliable method to determine the association rate constant, because it analyses only the early stages of binding. For rather stable complexes like a hybrid of two 15mer oligonucleotides with zero mismatch, a 10 min rinsing phase is not sufficient to see a significant dissociation that can be analyzed quantitatively. However, it is very well suited to obtain the dissociation rate in the case of a single base mismatched double strand during the rinsing step, resulting in a visible loss of fluorescence intensity that allows for a quantitative determination of k_{off} in addition to k_{on}, and hence can also give the affinity constant K_A.

The typical titration experiment allows for the determination of the Langmuir adsorption isotherm and, hence, the affinity constant K_A based on the evaluation of surface coverages. However, by increasing the concentration and, hence, the occupancy of the probe binding sites, the interface is more and more charged resulting (at the low ionic strength used in these experiments) in an increasingly significant Coulombic barrier for the hybridization at the sensor surface. As a consequence, the (averaged) affinity constant can be significantly lower than that found by the global analysis or by kinetic-titration experiments at low bulk concentrations (relative to $K_d = K_A^{-1}$), i.e., low surface coverages.

The kinetic and equilibrium coverage measurements that are done in the kinetic-titration experiment clearly revealed the influence of the interfacial charging effect. For each concentration c_0 of the bulk solution, the association and dissociation of the target to and from the sensor surface can be quantified and then also an apparent (concentration dependent) affinity constant can be determined. This was demonstrated for the RR-15 oligonucleotide target solution, but was also clearly visible in the concentration dependent k_{on} rate constant (and hence the K_A values derived from that) obtained in the kinetic-titration experiment.

One should point out again that this dependence could be largely reduced by either using a diluted probe matrix or by

operating at a higher ionic strength in the buffer that screens the charges and hence allows for a cross-talk-free determination of reaction rates and affinity constants.

Finally, it is interesting to compare the rate constants and affinity constants for the RR-15 oligonucleotide and the RR-169 amplicons, which contain the identical recognition sequence fully complementary to the PNA catcher at the sensor surface somewhere in the middle of the single strand (cf. Table I). The differences are marginal compared, e.g., to the striking effect of a single mismatch introduced in the RR-mis-15 oligonucleotide target. This is somewhat surprising given the fact that upon the binding of a single RR-169 amplicon 169 charges are added to the interface, significantly higher than the 15 charges of an oligonucleotide RR-15. However, the stretching of the target at the low ionic strength used in these experiments (10 mM PB) leads to a thicker oligoelectrolyte layer, but not necessarily to a higher (spatial) charge density.

ACKNOWLEDGMENTS

[1] P.-E. Nielsen, M. Egholm, R.-H. Berg, and O. Buchardt, Science **254**, 1497 (1991).
[2] M. Egholm *et al.*, Nature (London) **365**, 566 (1993).
[3] P.-E. Nielsen and L. Christensen, J. Am. Chem. Soc. **118**, 2287 (1996).
[4] A. Mugweru, B.-Q. Wang, and J. Rusling, Anal. Chem. **76**, 5557 (2004).
[5] L.-A. Bottomley, M.-A. Poggi, and S.-X. Shen, Anal. Chem. **76**, 5685 (2004).
[6] T.-H. Ha, S. Kim, G. Lim, and K. Kim, Biosens. Bioelectron. **20**, 378 (2004).
[7] W. Knoll, Annu. Rev. Phys. Chem. **49**, 565 (1998).
[8] T. Liebermann, W. Knoll, P. Sluka, and R. Herrmann, Colloids Surf., A **169**, 337 (2000).
[9] T. Liebermann and W. Knoll, Colloids Surf., A **171**, 115 (2000).
[10] K. Vasilev, W. Knoll, and M. Kreiter, J. Chem. Phys. **120**, 3439 (2004).
[11] J. Spinke, M. Liley, H.-J. Guder, L. Angermaier, and W. Knoll, Langmuir **9**, 1821 (1993).
[12] W. Knoll, H. Park, E.-K. Sinner, D. Yao, and F. Yu, Surf. Sci. **570**, 30 (2004).
[13] L.-D. Roden and D.-G. Myszka1, Biochem. Biophys. Res. Commun. **225**, 1073 (1996).
[14] N.-J. Mol, E. Plomp, M.-J.-E. Fischer, and R. Ruijtenbeek, Anal. Biochem. **279**, 61 (2000).
[15] T.-A. Morton, D.-G. Myszka1, and I.-M. Chaiken, Anal. Biochem. **227**, 176 (1995).
[16] D. Kambhampati, P.-E. Nielsen, and W. Knoll, Biosens. Bioelectron. **16**, 1109 (2001).
[17] K. Tawa and W. Knoll, Nucleic Acids Res. **32**, 2372 (2004).
[18] W. Knoll, M. Liley, D. Piscevic, J. Spinke, and M.-J. Tarlov, Adv. Biophys. **34**, 231 (1997).
[19] A. Germini, A. Zanetti, C. Salati, S. Rossi, and R. Marchelli, J. Agric. Food Chem. **52**, 3275 (2004).
[20] A. Germini, A. Mezzelani, F. Lesignoli, R. Corradini, R. Marchelli, R. Bordoni, C. Consolandi, and G.-D. Bellis, J. Agric. Food Chem. **52**, 4535 (2004).
[21] A. Germini, S. Rossi, A. Zanetti, R. Corradini, C. Fogher, and R. Marchelli, J. Agric. Food Chem. **53**, 3958 (2005).
[22] F. Lesignoli, A. Germini, R. Corradini, S. Sforza, G. Galaverna, A. Dossena, and R. Marchelli, J. Chromatogr., A **922**, 177 (2001).
[23] T. Neumann, M.-L. Johansson, D. Kambhampati, and W. Knoll, Adv. Funct. Mater. **12**, 575 (2002).
[24] F. Yu, D. Yao, and W. Knoll, Nucleic Acids Res. **32**, e75 (2004).
[25] D. Yao, F. Yu, J. Kim, J. Scholz, P.-E. Nielsen, E.-K. Sinner, and W. Knoll, Nucleic Acids Res. **32**, e177 (2004).
[26] D. Yao, J. Kim, F. Yu, P.-E. Nielsen, E.-K. Sinner, and W. Knoll, Biophys. J. **88**, 2745 (2005).